Materials Science and Engineering R 70 (2010) 209–224

Contents lists available at ScienceDirect

Materials Science and Engineering R

journal homepage: www.elsevier.com/locate/mser

Principles and applications of micro and nanoscale wrinkles

Yongfeng Mei [a,b,*], Suwit Kiravittaya [a], Stefan Harazim [a], Oliver G. Schmidt [a]

[a] Institute for Integrative Nanosciences, IFW Dresden, Helmholtzstrasse 20, D-01069 Dresden, Germany
[b] Department of Materials Science, Fudan University, Shanghai, 200433, Peoples's Republic of China

ARTICLE INFO

Article history:
Available online 29 June 2010

Keywords:
Wrinkle
Rolled-up Nanotech
Nanochannel
nanofluidics
Graphene

ABSTRACT

In this review, we summarize recent and interesting applications of micro and nanoscale wrinkles. Fluidic studies are comprehensively highlighted for various wrinkled nanochannels. Wrinkling as a mechanical characterization tool is also explained. As a new feature, wrinkles are employed to modify structures or physical properties of nanomaterials. It is promising to apply wrinkling for strain-engineering of graphene. We believe that wrinkling offers entirely new research perspectives in micro and nanotechnologies as well as in material sciences and engineering.

© 2010 Elsevier B.V. All rights reserved.

Contents

1. Introduction . . . 209
1.1. Wrinkles . . . 209
1.2. Wrinkles in micro and nanotechnologies . . . 211
1.3. Overview . . . 211
2. Wrinkles for micro and nano-fluidic applications . . . 212
2.1. Wrinkled-up micro/nanochannels by releasing semiconductor layers . . . 212
2.1.1. Deterministic fabrication of wrinkled-up micro/nanochannels . . . 212
2.1.2. Self-assembly of two-dimensional micro/nanochannel networks . . . 214
2.1.3. Release and bond-back effect in channel formation . . . 214
2.1.4. Strain and optical properties of individual wrinkled micro/nanochannels . . . 215
2.1.5. Fluidic behavior in wrinkled micro/nanochannels . . . 216
2.2. Wrinkles on surface-treated plastic substrates for elastic nanochannels . . . 217
2.2.1. Nanochannel formation on plasma-oxidized PDMS substrates . . . 217
2.2.2. Tunable fluidic nanochannels for particle and DNA manipulation . . . 218
2.3. Wrinkled surfaces as micro/nanofluidic templates and sieves . . . 218
2.3.1. Basic principles of wrinkled templates and sieves . . . 218
2.3.2. Reversible wrinkling for controllable transfer of colloidal patterns . . . 220
3. Wrinkling for mechanical characterization at micro/nanoscales . . . 220
3.1. Buckling-based metrology . . . 220
3.2. Capillary wrinkling . . . 221
4. Wrinkling as a new feature in nanostructures . . . 221
4.1. Wrinkled one-dimensional nanostructures . . . 221
4.2. Wrinkled-up graphene for strain-engineering . . . 222
5. Conclusions and outlook . . . 223
Acknowledgements . . . 223
References . . . 223

1. Introduction

1.1. Wrinkles

A wrinkle can be a fold, ridge or crease in the skin and normally appears when one becomes old. It thus enables a huge market for

* Corresponding author.
E-mail address: y.mei@ifw-dresden.de (Y. F. Mei).

0927-796X/$ – see front matter © 2010 Elsevier B.V. All rights reserved.
doi:10.1016/j.mser.2010.06.009

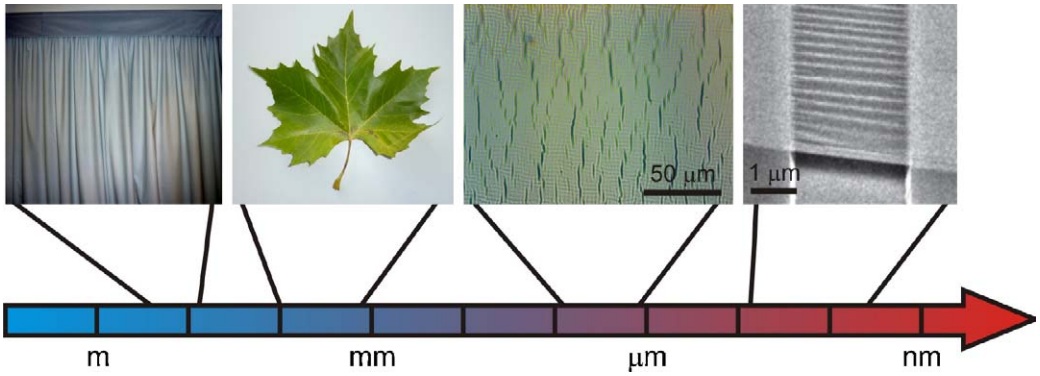

Fig. 1. Observation of wrinkling phenomena in nature. The dimensions (periodicity and amplitude) of wrinkles span across many length scales (from meters to nanometers). For example: (from left to right) a hanging-down curtain, a drying leaf, Al_2O_3 thin films on PDMS substrate, and stretched graphene sheets [1]. Reprinted with permission from Macmillan Publishers Ltd.: *Nature Nanotechnology* [1], copyright (2009).

anti-wrinkle cream etc. Although such wrinkles are very critical for the skin of human beings, wrinkling is a very general phenomenon in nature with dimensions (like periodicity and amplitude) spanning across length scales from meters down to nanometers. Basically, when a layer or sheet is forced to extend or shrink in its plane, it will be wrinkled or buckled in the perpendicular direction if there is limited planar space due to certain geometrical boundary conditions. As shown in the first image of Fig. 1 (from left to right), a curtain hanging down from the ceiling assumes a wrinkled shape on the decimeter scale since the curtain sheet is geometrically constrained in the plane. In the second image, when a leaf drops down to the ground, it dries out and experiences a centimeter-scale buckling at the edge, which is similar to human skin wrinkling or dried wizen fruits. In conventional thin film deposition technology, delaminated films often show buckles (wrinkles or blisters) due to the high compressive stress. As illustrated in the third image of Fig. 1, a thin oxide film deposited on a *poly-(dimethyl)siloxane* (PDMS) substrate shows a regular pattern of wrinkles at a scale of microns after cooling down. Here, the wrinkling is mainly due to the different thermal expansion coefficients between oxides and plastic. People have also created nanoscale wrinkles or buckles with the aim to change the electronic properties of materials. As shown in the right image of Fig. 1, a graphene sheet is wrinkled by controlled thermal treatment, which might open a way to strain-engineer a bandgap in graphene [1].

The study of wrinkles interacts with many other scientific disciplines and establishes a technological platform for plenty of interdisciplinary research. It has been observed by George M. Whitesides that wrinkling of thin metal films on PDMS substrates can be used to create ordered microstructures [2]. After that, a lot of effort has been dedicated to study and understand wrinkled pattern formation [3,4]. Theoretically, wrinkling involves large deformations of thin flat sheets whose behavior is governed by a set of non-linear partial differential equations, known as the Föppl-von Karman equations [5]. In general, these equations cannot be solved analytically except in some one-dimensional cases. Since this topic has been extensively reviewed previously [3,4], we will not focus on the quantitative pattern formation, itself. Instead, we concentrate on the underlying principles and applications of micro and nanoscale wrinkles, leaving out extensive theoretical modeling and computation. We expect that our topical review will be helpful to elucidate the huge application potential of wrinkles in micro and nanotechnologies.

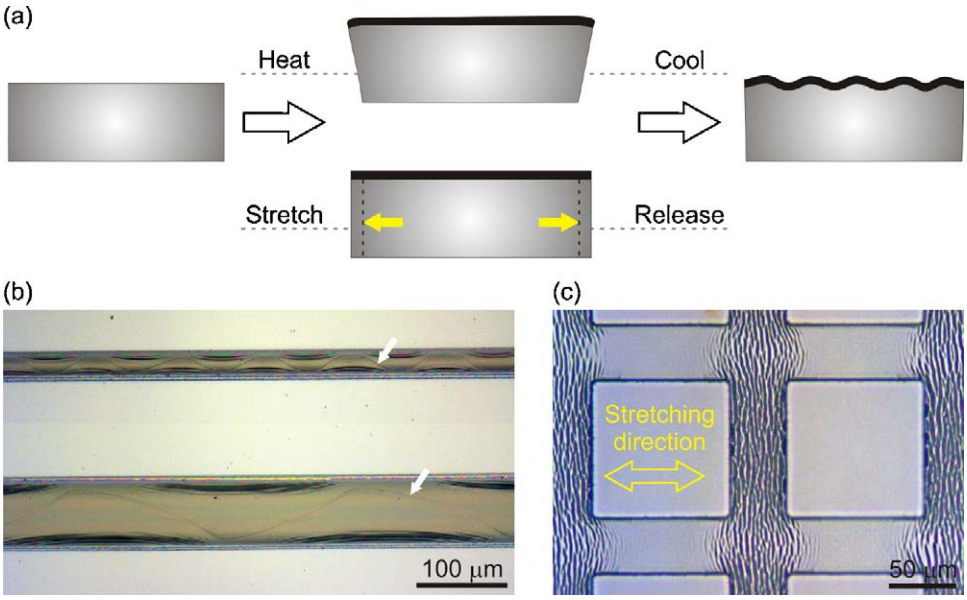

Fig. 2. (a) Procedures for wrinkling on PDMS. The PDMS substrates are heated or stretched for volume expansion and subsequently coated with thin layers. Upon cooling or releasing, the coated layers form wrinkled patterns. (b) Wrinkled patterns exhibit a sinusoidal feature for Al_2O_3-coated photoresist layers fabricated by atomic layer deposition by using the principle of heating and cooling shown in (a). (c) Wrinkled patterns formed by stretching, Al_2O_3 coating and relief of a PDMS substrate.

1.2. Wrinkles in micro and nanotechnologies

For the development of micro and nanotechnologies, one of the most important questions is how to create regular micro and nanostructures over a large area in a simple and efficient way, which then enables these technologies to be transferred to industry-relevant applications. Researchers have developed several promising techniques, such as nano-imprinting [6], template-assistance [7–9], self-assembly [10] etc., to generate micro/nanostructures and their arrays on a large area. In 1998, it was found that complex and ordered micro/nanostructures can be formed by the buckling of thin metal films owing to thermal contraction of an underlying substrate by Bowden et al. [2]. As shown in Fig. 2a, the films are deposited onto a thermally expanded polymer sheet, and subsequent cooling of the polymer creates compressive stress in the deposited film, which then is relieved by wrinkling or buckling with uniform periodicity. Several reviews have summarized current achievements in the formation of wrinkled patterns [3,4,11,12]. Without well-defined boundary conditions, a metal film on a polymer substrate, e.g. PDMS, forms into a random wrinkle pattern. Therefore, regular shapes like strips or disks are often designed to achieve well-ordered arrays of micro/nanostructures. One interesting method is to apply conventional photolithography to pattern photoresist layers and initiate the wrinkling process to such patterned polymers. For example, after coating of a 20 nm thick Al_2O_3 layer by atomic layer deposition, the wrinkled patterns created by deposition exhibit a sinusoidal feature as shown in Fig. 2b, as well as plastic deformation by crack formation (see white arrows). Wrinkling can be also realized by stretching and releasing (bottom part of Fig. 2a) the polymer sheet, which is similar to the heating and cooling process outlined in the top part of Fig. 2a. In Fig. 2c, squares are defined on a PDMS substrate by using more than 2-μm thick photoresist. After thin film deposition on the stretched substrate, the substrate and the film are released. Wrinkled patterns arise only along the perpendicular direction of the stretching direction, which illustrates that stretching and releasing can control wrinkled pattern formation in a directional way different to the heating and cooling process.

Another exciting research field related to wrinkles in micro and nanotechnologies is stretchable electronics realized by inorganic semiconductors [14]. We briefly describe several features here as it has been well reviewed somewhere else [13–15]. This field is mainly advanced by the group of John A. Rogers at the University of Illinois at Urbana-Champaign. Such systems integrate inorganic electronics materials, including aligned arrays of nanoribbons of single crystalline silicon with plastic and elastomeric substrates. The buckled (or wrinkled) [16] or "wavy" [17] configurations of functional circuits facilitate the whole systems to be stretchable and bendable for remarkable device applications like deformable and semitransparent displays [18], hemispherical electronic eye imagers [19], and cardiac and brain monitoring devices [20]. In the buckled (or wrinkled) case, the approach involves the combined use of two-dimensional lithography to provide spatial control over adhesion sites and elastic deformations of a supporting substrate to induce well-controlled local displacement for the wrinkled nanoribbons [16]. As shown in Fig. 3a, precisely engineered buckled geometries are created from Si nanoribbons on a PDMS substrate [16]. The image shows the variation of the amplitudes with change in wavelength of the wrinkled nanoribbons. In the case of "wavy" configurations, the design combines multilayer neutral mechanical plane layouts with the wrinkled shapes of silicon circuits [17]. Fig. 3b illustrates this type of fully optimized, dual neutral mechanical plane layout and its ability to be stretched or bent. The optical micrographs at the bottom left and right demonstrate the various configurations observed under extreme twisting and stretching of the system. In order to reach extreme bending (i.e. folding) or extreme twisting, an encapsulating layer is employed to meet both requirements, but with different materials as described in ref. [17]. The combination of both "wavy" and buckled configurations offers even more flexibility and promise numerous significant applications including electronic eyeball cameras and personal health monitors.

Besides the fields described above, wrinkled micro/nanostructures are being pursued for many unique applications in e.g. fluidics, mechanical metrology, and strain-engineering. In this review, we highlight the potential applications of wrinkles and focus on materials science and engineering of wrinkles on a small scale.

1.3. Overview

We review very recent developments of micro and nanoscale wrinkles. In Section 1, a general introduction is given. In Section 2, wrinkles for micro and nanofluidic applications are comprehensively reviewed in three subsections: (i) wrinkled-up micro/nanochannels by releasing semiconductor layers; (ii) wrinkles on surface-treated plastic substrates for elastic nanofluidic channels; (iii) wrinkled surfaces as micro/nanofluidic sieves or templates. In Section 3, a wrinkling phenomenon, which is used for mechanical

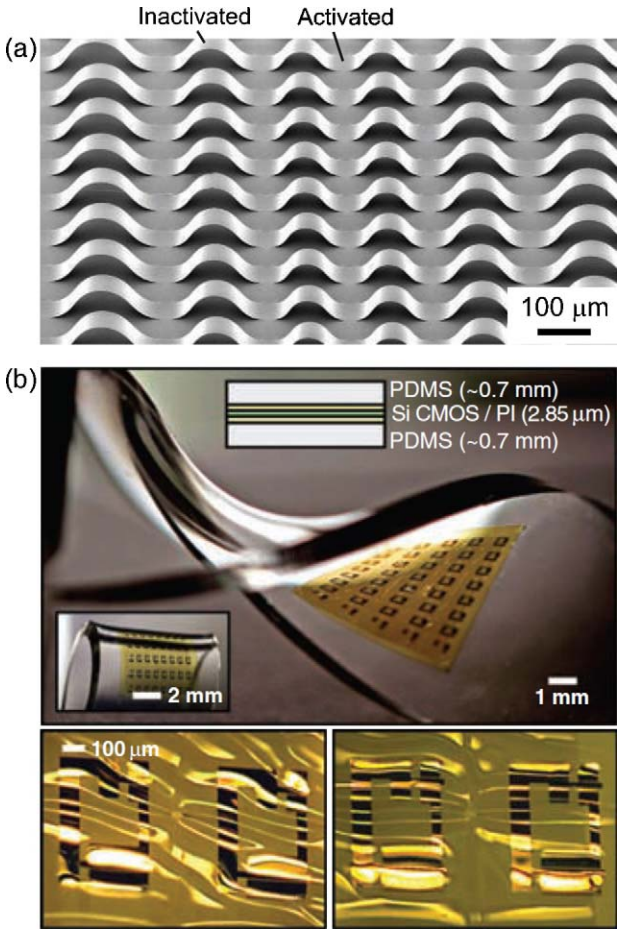

Fig. 3. (a) Si nanoribbons formed on PDMS substrate pre-strained by 50% and patterned with 15 μm wide activated stripes and 350, 300, 250, 250, 300, and 350 μm (from left to right) wide inactivated stripes [16]. (b) Images of twisted (top) and bent (bottom inset) wavy Si-CMOS circuits that use a dual neutral plane design. The inset at the top shows a coarse cross-sectional view. Optical micrographs of inverters at the center (bottom left) and edge (bottom right) of the sample in the twisted configuration are shown in the top frame [17]. Reprinted with permission from AAAS.

characterization at micro/nanoscales, is described. An interesting application of capillary wrinkling for local detection of mechanical properties of plastic sheets will be explained. As a new modification of nanostructures, wrinkling in one- and two-dimensional nanostructures will be presented in Section 4, where strain-engineering is an important feature for new physics. Finally, conclusions and an outlook are given for possible directions in both fundamental and application related research.

2. Wrinkles for micro and nano-fluidic applications

2.1. Wrinkled-up micro/nanochannels by releasing semiconductor layers

2.1.1. Deterministic fabrication of wrinkled-up micro/nanochannels

Micro/nanochannels formed by wrinkled semiconductor nanomembranes are described in this subsection. The release of a semiconductor layer from the substrate is carried out by sacrificial layer etching techniques. The film structure consists of the mother substrate, sacrificial layer, and strained nanomembrane for wrinkling. Conventional semiconductor materials (Si or GaAs) are typically used as substrates depending on the type of strained nanomembranes, and a removable layer denoted as a sacrificial layer is sandwiched between substrate and nanomembranes. The semiconductor materials used here can easily be integrated with other electrical and optical systems like transistor circuits for sensing and optical components for light emission sources. The functional nanomembrane wrinkles can be composed out of compound crystalline semiconductor materials like $Si_{1-x}Ge_x$ or $In_{1-x}Ga_xAs$, which can be grown by molecular beam epitaxy (MBE) or metal-organic chemical vapor deposition (MOCVD) in a defect-free manner. Well-controlled lattice mismatch leads to predictable and reproducible homogeneous strains in these nanomembranes. Here we use two types of material systems: SiGe-on-insulator (SiO_2), where the SiGe layer acts as a pre-strained nanomembrane for wrinkling and SiO_2 as a sacrificial layer; and InGaAs and AlAs, where the InGaAs layer serves for wrinkling and AlAs is the sacrificial layer. SiO_2 and AlAs can be selectively etched away due to their high chemical selectivity to hydrofluoric acid (HF) in even very dilute concentration. A strained nanomembrane can either wrinkle or bend upon release, depending on the built-in differential stress across the nanomembrane thickness [21]. A large strain gradient across the thickness induces rolling of the membrane, while a lower strain gradient with high average strain and longer etching depth leads to wrinkling [21]. Once the wrinkle has formed it can be characterized by the wrinkle amplitude A and the wrinkling wavelength λ, both depending on the etching depth h. The relaxation by wrinkle formation lowers the total elastic strain energy in the deformed membrane structure. Raman scattering spectroscopy is used to probe the strain state in the structure. The Raman data from the SiGe-on-insulator nanochannel are given in Fig. 4a. The inset shows how wrinkled nanochannels are formed by selectively etching away the SiO_2. The change of strain in the $Si_{1-x}Ge_x$ layer before and after the "release and bond-back of the layers" (REBOLA) was measured by micro-Raman scattering [22]. The red curve represents the Raman spectrum of the strained SiGe nanomembrane before under-etching. The peak at 520 cm^{-1} stems from the first-order longitudinal optical phonon Si–Si vibration mode of the Si substrate, whereas the peak at 512 cm^{-1} originates from the Si–Si vibration mode of the compressively strained SiGe layer. The blue spectrum was taken from an already bonded back area where

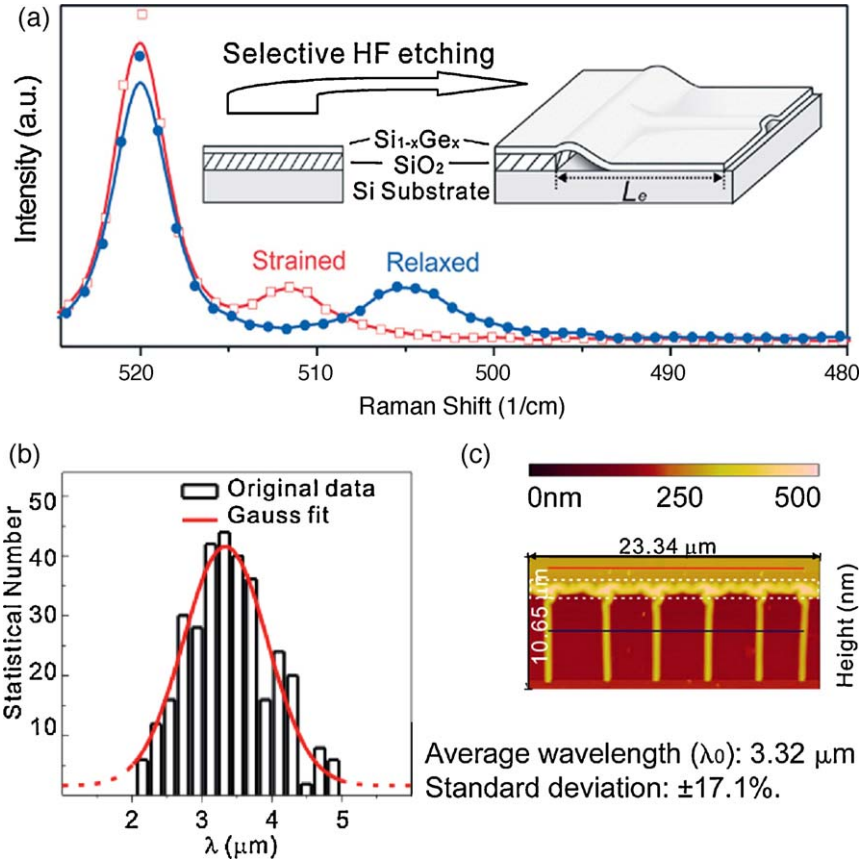

Fig. 4. Properties of an ultrathin $Si_{1-x}Ge_x$ film on a 100 nm thick SiO_2 layer (a) Raman spectra of a strained and relaxed layer. The inset shows a schematic illustration of the formation of the $Si_{1-x}Ge_x$ channel structure by HF etching of SiO_2 [22]. (b) Statistical distribution of the wrinkling wavelength λ_0 with an average of 3.32 μm for SiGe layers. (c) Atomic force microscopy (AFM) image of the linear wrinkled network [22].

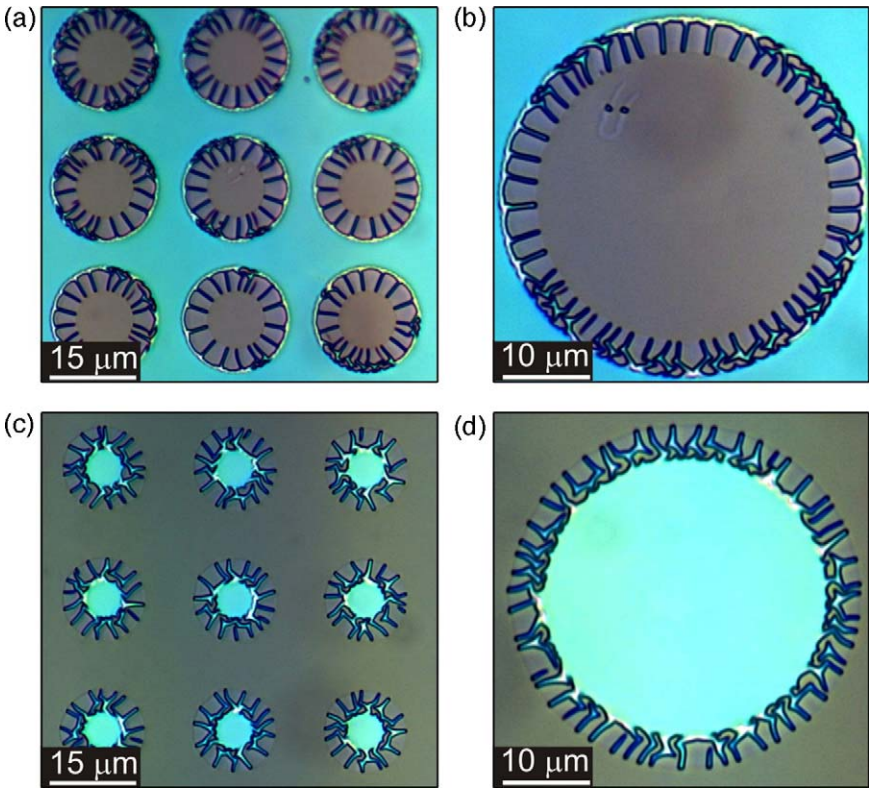

Fig. 5. Examples of deterministic wrinkled circular channel networks. (a–b) Wrinkled channels from strained nanomembranes with patterns of circular etched holes. After etching of the sacrificial layer, circular channel networks occur together with branch channels. (c–d) Wrinkled channels from strained nanomembranes with defined circular patterns. The bright blue central structure is still unetched with a sacrificial AlAs layer underneath.

the SiGe layer touches the Si substrate surface directly. The Si–Si vibration mode of this SiGe layer is shifted by 7 cm^{-1} compared to the strained SiGe layer. A Ge composition of 24% and a 1.1% compressive strain in the $Si_{0.76}Ge_{0.24}$ film before etching was calculated [22]. The degree of relaxation can also be calculated by measuring the surface point-to-point distance difference of the original flat layer and relaxed wrinkled surface. The standard deviation of the wrinkle periodicity is statistically calculated as 17.1% (Fig. 4b), and the average wavelength is $\lambda_0 = 3.32$ μm. An atomic force microscopy (AFM) image of a wrinkled nanomembrane surface is presented in Fig. 4c: the red line scan was taken on the planar and unetched surface, and the blue line scan along the wrinkled area. The blue line path integration across the wrinkled area results in a 1.187% longer distance than the length of the red line scan across the flat surface area. The agreement of the strain measurement by both micro-Raman spectroscopy and the line scan method is good. The slight difference of both methods can be explained by the inhomogeneous strain across the thin SiGe nanomembrane in the vertical direction, and/or the non-equidistance between each branch channel pair [22,23].

The deterministic wrinkling of strained layers enables us to create well-defined wrinkled nanochannel networks. The effective channel diameter can vary from a few tens of nanometers to several hundred nanometers [22,24]. Depending on the built-in strain a large range of wrinkled channel sizes and wrinkling wavelengths are possible. By defining the start window for etching by photolithography, different nanochannel networks can be formed like linear and circular shapes. For example, with positive

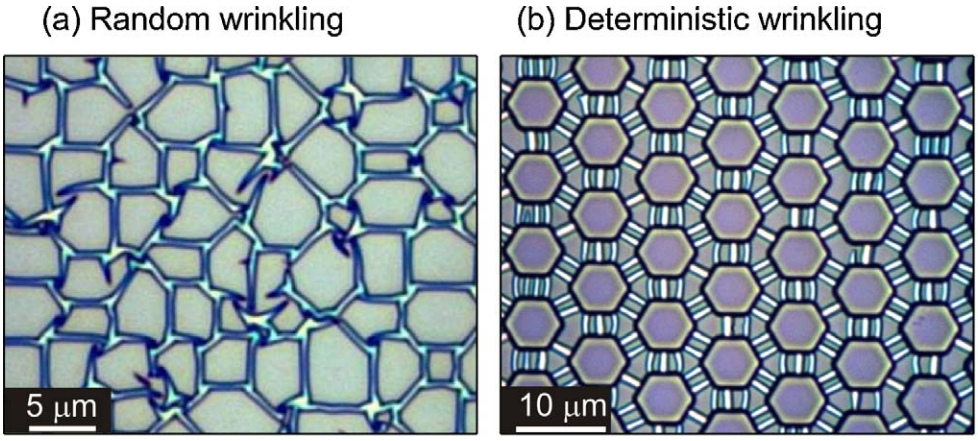

Fig. 6. Random versus deterministic wrinkling. (a) Random wrinkles from the strained nanomembrane underetched without deterministic control. (b) Ordered channel network from strained nanomembranes with a designed pattern for undercut.

and negative patterning, circular wrinkled nanochannel networks can be formed from inside or outside the pattern after etching. The optical microscopy images in Fig. 5 provide examples of how hole (Fig. 5a and b) and mesa structures (Fig. 5c and d) lead to circular nanochannel networks. The sacrificial layer is selectively removed by a diluted HF solution. The length of the wrinkled branch nanochannels corresponds to the HF etching time. The number of branch channels is given by the ratio between circular perimeter and the wrinkling wavelength of the predefined structure.

2.1.2. Self-assembly of two-dimensional micro/nanochannel networks

In Section 2.1.1, one-dimensional linear and circular micro/nanochannel networks were discussed. But what happens if strained nanomembranes are simultaneously released in two dimensions? By underetching a strained nanomembrane with a large area (larger than the wrinkling wavelength in lateral dimensions), the entire released membrane can fold and relax randomly as shown in Fig. 6a. However, when an array of hexagonally shaped windows is defined by photolithography, the self-assembly of micro/nanochannel networks can be well controlled and two-dimensionally ordered channel networks are formed as shown in Fig. 6b. The hexagonal start windows have an inter-distance comparable to the maximal straight channel length [24], which is a key for the realization of a highly ordered wrinkled micro/nanochannel network.

Besides possible control of intrinsic parameters, extrinsic parameters like size of start windows, inter-distance between start windows, strain and thickness in pre-strained nanomembranes can also be adjusted. Fig. 7a summarizes graphically the configuration space range that was investigated for square and hexagonally patterned networks made of 10 and 20 nm thick $In_{0.2}Ga_{0.8}As$ layers [24]. An indicator of the network quality is represented by the size and aspect ratio of the colored circles in the diagram. Three classes were established: "completely ordered" if all pits are connected by one or more direct channels; "mostly ordered" if less than 25% channel links are missing, broken, or connecting more than one pit; and "poorly ordered networks" with more than 50% defects. Missing points in the diagram denote configurations that lead to completely disordered channels or are geometrically forbidden. From the diagram, we conclude that square networks exhibit a better quality for large starting windows (side-length: w) and relatively small hole periodicity (inter-distance: l). The best ordering for the hexagonal networks was found at intermediate w values and large l. The two arrows labeled A and B in the configuration diagram represent typical paths for the wrinkling behavior under different w and l conditions. The optical images of the network fields along those paths are shown in Fig. 7b. Along path A the networks undergo a transformation from completely random at $w = 1\ \mu m$ to mostly ordered at $w = 4\ \mu m$. Wrinkling with thinner InGaAs membranes leads to more complex multidirectional wrinkles. The evolution of the ordering in hexagonal networks along path B is also shown in detail in Fig. 7b. In the hexagonal networks, longer channel distances are easily obtained as a result of the larger channel density, which is tied to the availability of pit edges and the possibility of multichannel creation. Single and multichannel preferences can be explained by the in-plane relaxation constraint caused by the lithographic template edges. Since these templates comprise a square area of $100\ \mu m \times 100\ \mu m$, there is a limited lateral extent for the bonding-back of the released film [24]. However, future studies on the channel formation on different template sizes will be very important for the understanding and control of ordered wrinkled channel formation.

2.1.3. Release and bond-back effect in channel formation

Wrinkles are often assumed to have a sinusoidal shape with a smooth variation in geometry [12] but in our case there is plenty of flat space between the wrinkled channels. By carefully checking the wrinkled nanomembrane in liquid prior to the drying process, it is found that the geometry of the wrinkled nanomembranes (SiGe-on-insulator system) in liquid are rather different from that in the dried state as shown in Fig. 8a (in liquid) and b (after drying). One can understand this difference by considering the bond-back effect of wrinkled nanomembranes during drying, which is driven by the liquid surface tension. If one attempts to model the whole system, the ideal situation for wrinkled nanomembranes in liquid is illustrated as the top schematic in Fig. 8c. Apart from the initial strain and the thickness of the pre-strained nanomembranes, there are two competing parameters: the amplitude of the wrinkles and

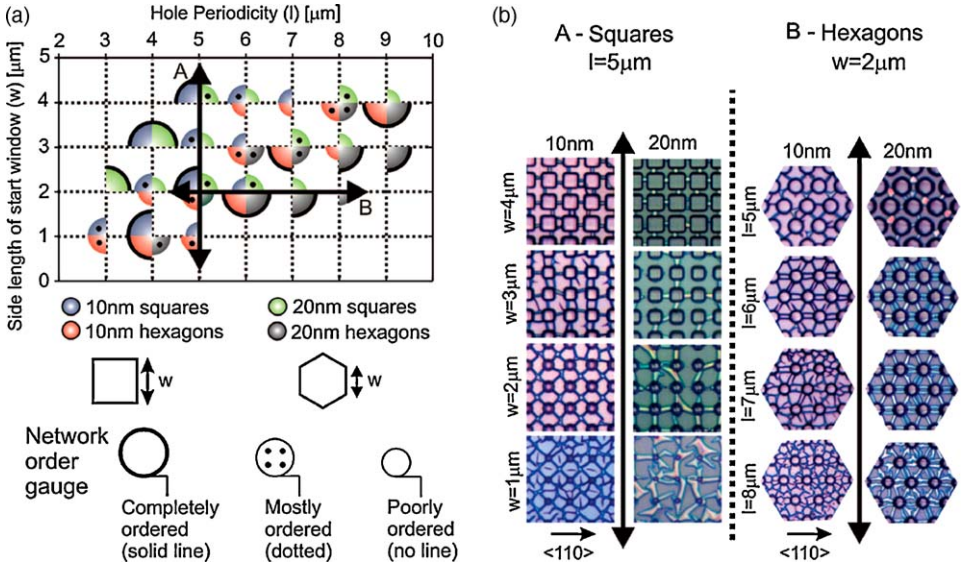

Fig. 7. (a) Graphical representation of the configuration space range tested for obtaining square and hexagonally ordered networks in 10 and 20 nm thick $In_{0.2}Ga_{0.8}As$ films. A semi-quantitative gauge is used to index the obtained network order. The pit edge width defined here is shown for each shape [24]. (b) Optical images of the obtained channel patterns for two paths along the configuration space are shown for fixed square hole periodicity (arrow A) and fixed hexagon window size (arrow B) [24]. Reprinted with permission from [24].Copyright 2008 American Chemical Society.

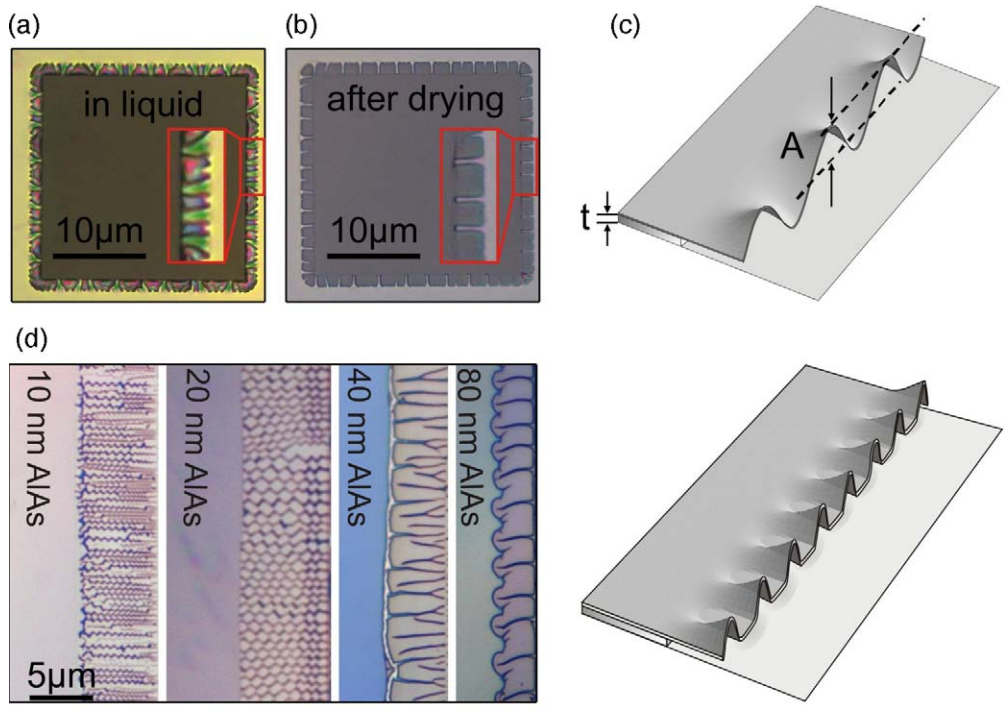

Fig. 8. The bond-back effect. Optical images of a wrinkled nanomembrane (a) in a liquid after etching and (b) after drying. (c) Schematic drawing to point out how the bond-back effect is influenced by the amplitude (A) of wrinkles and the sacrificial layer thickness (t). (d) Periodicity and geometry of wrinkles as a function of the thicknesses of sacrificial layers (labeled in images).

the height of the sacrificial layer, which directly influence the final geometries of the micro/nanochannels (lower image of Fig. 8c). As we know, the amplitude of wrinkles increases with etching length [22]. We choose 10 nm thick InGaAs nanomembranes on an AlAs sacrificial layer with various thicknesses of 10, 20, 40, and 80 nm. By selectively etching away the AlAs layers, the wrinkled channels assume different geometries. Fig. 8d shows that for 80 nm AlAs sacrificial layers, the wrinkles form into well-isolated channels as reported before [23,24]. When decreasing the AlAs sacrificial layer thickness to 40 nm, the wrinkles assume a two sub-channel like Y shape reaching from the etching front to the start edge. The size of the channels is reduced as well. When further thinning the AlAs layer down to 20 nm, channels transform into zigzag shapes and shrink in size. Finally, when the AlAs thickness is reduced to 10 nm, the channels preserve the zigzag shape but become even smaller. The interpretation for these phenomena is straight-forward: For a thin sacrificial layer, wrinkles with small amplitudes interact with the substrate surface already for a short etching width and hence the wrinkled channels become smaller than for membranes on thick sacrificial layers. As for the shape changes, the interaction between wrinkles and substrate during etching becomes more pronounced for thin sacrificial layers, eventually causing a behavior similar to conventional wrinkle formation in PDMS [2]. Such effect is simply called the maximal straight channel length [24], and thus the channel assumes a straight, Y-shaped, and zigzag shape as the sacrificial layer thickness is reduced at a fixed etching width. Our experiments prove that wrinkled channels are strongly influenced by the thickness of the sacrificial layer due to the interaction between the wrinkles and the substrates. It further reveals that the bond-back effect occurs both in liquid and upon drying, which results in various channel geometries.

2.1.4. Strain and optical properties of individual wrinkled micro/nanochannels

In Section 2.1.1, we have measured the average compressive strain in the wrinkled channel network. However, a study on individual channels (i.e. wrinkles) should provide more information on the strain state of wrinkled nanomembranes, which is caused by the bond-back effect. For this purpose, we embedded an InGaAs quantum well into a GaAs nanomembrane. Such a passivated quantum well acts both as a local strain sensor as well as a strain source [22]. Micro-photoluminescence spectroscopy was adopted to record and analyze the quantized states in wrinkled quantum wells.

Panel (a) in Fig. 9 shows schematic drawings of the lattice deformations and different strain states in an unetched nanomembrane and in a wrinkled structure including the bonded-back and the wrinkled region. The shift of the photoluminescence emission peak can be used to monitor the strain state in the layer after deformation since the strain affects the electronic structure of the wrinkled layer [22]. The left panel in Fig. 9a illustrates the intrinsic stress of the initial unreleased layer by arrows. In the bonded back state the layer was released from the substrate and then partially relaxes its internal strain. The tensile stress of the barrier layers (above and below the quantum well layer) is induced by the partial relaxation of the strain in the quantum well layer (middle panel in Fig. 9a). For the wrinkled case, the bending of the membrane produces an inhomogeneous strain distribution where the lattice constant along the growth direction depends on the inner lattice constant and the curvature and varies linearly with the distance from the inner wrinkle surface to the outer surface [23]. To obtain the residual forces, which can either be tensile or compressive as shown in the right panel of Fig. 9a, we assume a certain position for the neutral plane, which is defined as the plane where the resultant stress is zero (dotted line). The band edge diagram of the quantum well (QW) shown in Fig. 9b corresponds to each panel shown in Fig. 9a, and is calculated by taking into account the effects of strain using linear deformation potential theory. The calculated ground state transition energies as a function of curvature are given in Fig. 9c. The calculations include three different models for the wrinkle structure. The first model assumes strain energy minimization at predefined curvature (Bent

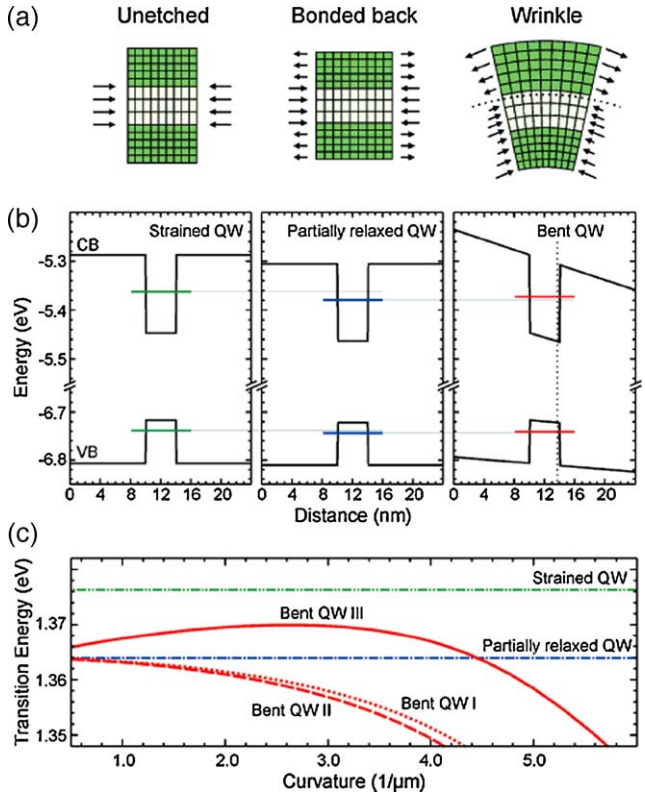

Fig. 9. Schematic of the unetched (strained QW), bonded back (partially relaxed QW) and wrinkle (bent QW) structures. (a) Arrows represent the force applied to the layer, and the dotted line in the wrinkle structure indicates the neutral plane. (b) Band edge diagrams which correspond to (a). The lines in the middle of the QW show the quantized energy levels of the electron in the conduction band (CB) and heavy hole in the valence band (VB). Light-gray lines are guides to the eyes. (c) Transition energy of the bent QW as a function of the bending curvature. The dashed–dotted-dotted and the dashed–dotted lines represent the transition energies of the strained QW and partially relaxed QW, respectively. Three bent QW models are presented (red lines) [23]. Reprinted with permission from [23].Copyright 2007 American Chemical Society (For interpretation of the references to color in this figure legend, the reader is referred to the web version of the article.).

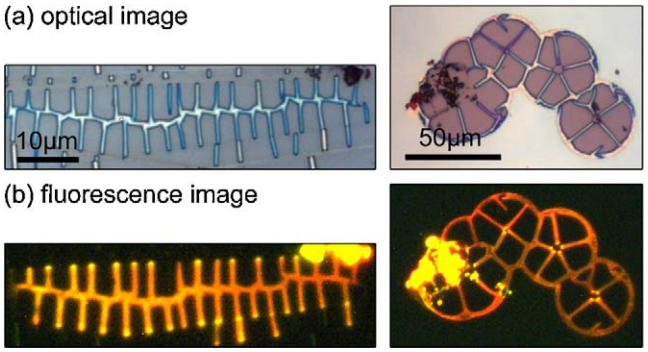

Fig. 10. Fluidic properties of wrinkled micro/nanochannel networks. (a) Optical image of a linear channel networks (left) and a channel network consisting of several circular ones (right). (b) Corresponding fluorescent images of (a) by using Rhodamine 6G as the fluorescent dye in solution. The bright yellow areas indicate the fluid input zone by a nanodroplet dispenser. The channels are filled due to capillary forces immediately. This indicates that the channels are firmly connected (For interpretation of the references to color in this figure legend, the reader is referred to the web version of the article.).

QW I). For the second model, the neutral plane is assumed to sit at the center of the QW layer due to the symmetric structure (Bent QW II), and a variable position of the neutral plane as a fitting parameter is considered in the third model (Bent QW III). From this calculation, we deduce that the obtained wrinkle experiences a complicated strain state, which is probably caused by external forces originating from the nearby bond-back area [23]. Upon drying, surface tensions at two interfaces (nanomembrane/liquid and substrate/liquid) push the relaxed nanomembrane onto the substrate and create additional strain inside in the wrinkled part of the channels.

2.1.5. Fluidic behavior in wrinkled micro/nanochannels

Depending on the surface characteristics and the properties of the fluid, simple fluidic transport experiments can be realized in our wrinkled micro/nanochannels. If the surface and the fluid show hydrophilic behavior then even nano channels can rapidly be filled with solvents due to the induced capillary forces. The nanochannel networks shown in Fig. 10 were defined by scratching the surface (Fig. 10a, left) or by point-like defects within the strained nanomembrane (Fig. 10a, right). By removing the sacrificial layer, the strained nanomembrane wrinkles to form long-range networks, with all single branch channels connected to each other. The interconnection of branch channels is easily revealed by adding a Rhodamine 6G dye solution locally to one spot of the network as shown in the fluorescent image in Fig. 10b. These fluorescent images correspond to the optical images shown in Fig. 10a.

The nanofluidic transport as well as the femtoliter filling and emptying characteristics of an individual wrinkle on a standard semiconductor substrate are shown in Fig. 11. A simplified brick-like geometry was considered to understand the observed fluid shape transitions during the fluid filling and emptying of a single wrinkle channel. Two different fluid shapes, which are given by the Young–Laplace relation, are considered (see insets of Fig. 11). The change in surface energy (E_{surf}) during channel filling and emptying is shown in Fig. 11. For shape 1 (upper right inset), the fluid is confined to one of the container walls while shape 2 (lower left inset) represents a square-like fluid plug that extends from one wall to the other. Due to the surface energy reduction, a fluid shape transformation at a certain critical volume can be explained [22]. Selected chronological video frames, concentrating

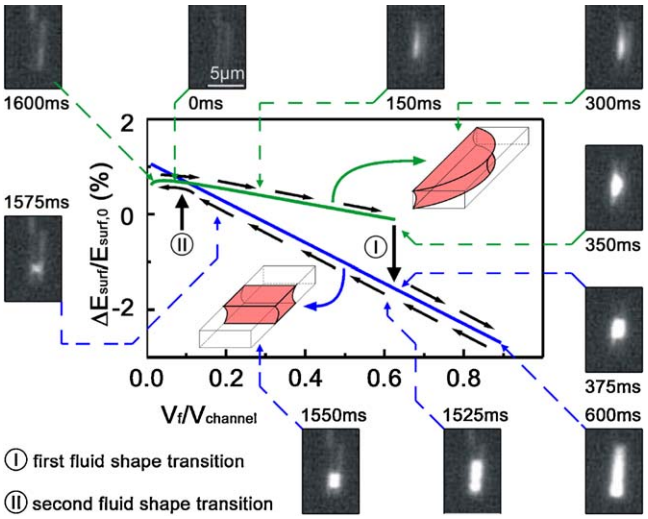

Fig. 11. The graph displays the surface energy as a function of fluid volume, in which the green line represents the arc-shaped fluid (upper right inset) and the blue line describes the rectangular-shaped fluid model (lower left inset). Surrounding insets are a series of selected video frames highlighting the transport behavior of fluid in a large wrinkle [22] (For interpretation of the references to color in this figure legend, the reader is referred to the web version of the article.).

on the filling and emptying process of the wrinkle, are given as insets in Fig. 11. The first frame at 0 ms was taken directly before filling of the wrinkle. From 0 to 350 ms, arc-like shapes of the fluid are observed in the wrinkle. From 375 to 1575 ms, rectangular shapes are formed during fluid filling and subsequent emptying. In the last frame (1600 ms), the arc shape appears again on the other side of the large wrinkle. This demonstrates the fluidic shape transition driven by minimization of the surface energy.

Nanochannel systems or even single channels can be used for the investigation of the fluid properties, themselves. Due to the small size new states of fluid manipulation are possible. The electric double layer (EDL) between a solid surface and an electrolyte solution has a thickness between roughly 1 and 100 nm, typically depending on the ion concentration in the solution. Compared to the bulk solution, the electrolyte is not electrically neutral within the EDL; therefore it can be manipulated by local electrical fields. The thickness of the EDL, the so-called Debye length, represents the shielding radius of ions in the solution. If this radius is comparable to the channel diameter the ion becomes 'visible' to an applied electric field. The electrical isolation of semiconductor-based wrinkled nanochannels can be achieved by using deposition methods like atomic layer deposition (ALD). The entire surface of a wrinkle is coated with a defined layer thickness using a convenient metal-oxide precursor. The fluidic behavior still exists after coating the channel surface with for instance an aluminum oxide layer, but with the additional effect of creating a pH depending surface potential. Due to the hydrophilic character of the metal oxide to water the fluid is driven into the channel by capillary forces. Furthermore, atomic layer deposition can be conveniently used to fine-tune the inner effective diameter of a wrinkled nanochannel.

Recent investigations have shown that it is possible to realize ion sensitive devices based on InGaAs wrinkled nanochannels [25]. The working principle of those devices relies on field-effect transistor (FET) operation, but the charge carriers are ions dissolved in a fluid instead of electrons in doped semiconductor layers. Due to easy parallel on-chip integration, this ion sensitive field-effect transistor (ISFET) based on wrinkled nanochannels can easily compete with recently developed ISFETs based on tubular structures, photolithographically defined nanochannels or even ion selective protein channels. Nanochannels made of wrinkled nanomembranes have atomically smooth surfaces since they are grown by MBE, which could solve problems arising from rough channel surfaces, which are severe in systems with relatively small channel sizes. Moreover, single crystalline nanomembranes like InGaAs or SiGe offer possibilities to integrate electrical and optical functions for novel semiconductor-based nanofluidic systems.

2.2. Wrinkles on surface-treated plastic substrates for elastic nanochannels

2.2.1. Nanochannel formation on plasma-oxidized PDMS substrates

Wrinkles can be created by deposition of various inorganic materials on stretched plastic sheets like PDMS, which we discussed in Section 1.2. In addition, oxygen plasma treatment can be introduced into the wrinkling process of PDMS. The process

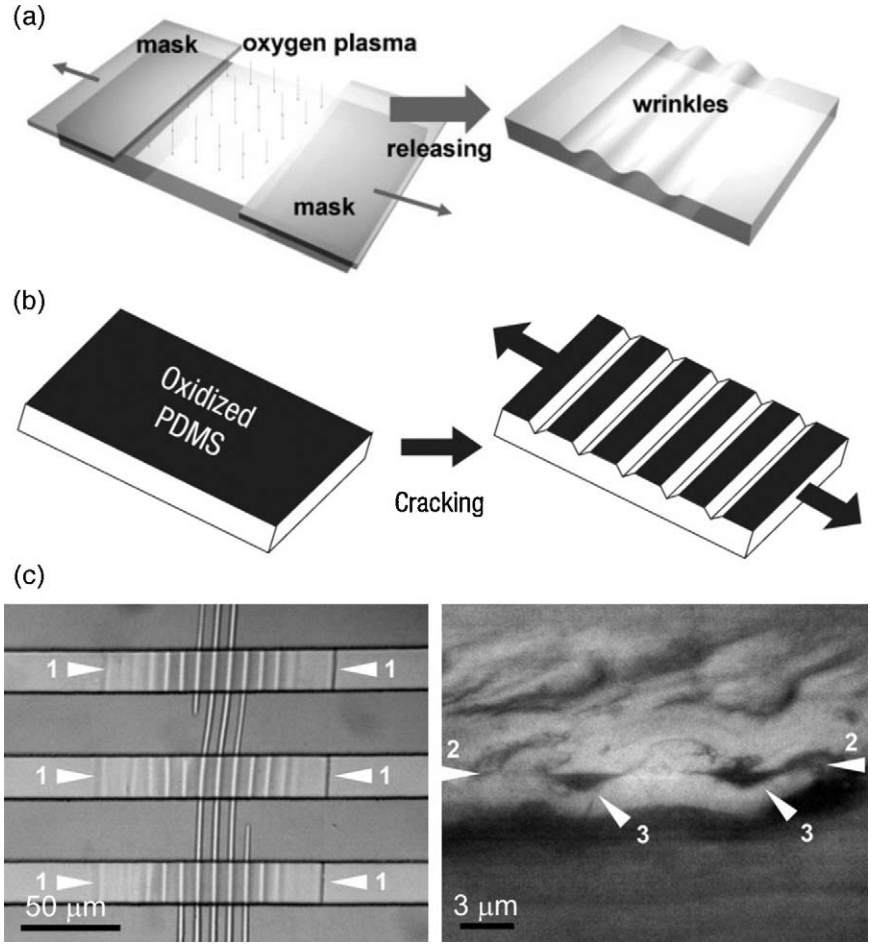

Fig. 12. (a) Sketches that mask-covered PDMS is exposed to oxygen plasma under uniform stretching (left), and wrinkles are formed after release (right) [28]. (b) PDMS substrate is treated with oxygen plasma and stretched to generate linear nanoscale cracks [30]. (c) Right image shows microfluidic channels matched with wrinkled nanochannels made by method (a), and the left image presents a magnified cross-sectional view of wrinkled nanochannels, revealing triangular cross-sections (arrow 3) [28].

includes (i) heating the PDMS for expansion; (ii) exposing the PDMS to oxygen plasma to generate a thin surface film of silica-like materials [26]; (iii) cooling down to generate the strain [27]. In this process, the oxygen plasma produces a thin silica-like film on the PDMS substrate, which acts as the functional deposited layer in Fig. 2a. By patterning the surface as shown in Fig. 12a, wrinkled structures are formed by selective exposure of the film to oxygen plasma [28]. The wavelength and amplitude of wrinkles can be independently controlled by varying strain (heating temperature) and time of plasma treatment. A higher temperature induces larger strain, thus leading to a larger amplitude of the wrinkles since the strain difference in the system does not influence the wrinkling wavelength [27]. An increase in exposure time can thicken the silica-like layers and affects both the wavelength and amplitude. However, from our point of view, a high heating temperature may not only induce larger strain but also accelerate the reaction of PDMS into silica-like materials during oxygen plasma treatment. It thus can thicken the silica-like layers and hence change the wavelength as well. Employing this method, nanochannels are manufactured by bonding the wrinkled surface to a planar microfluidic device. Such wrinkles can be used to fabricate arrayed nanochannels in a simple, one-step, and cost-effective process compared to other direct or imprint lithographic techniques.

As shown in Fig. 12b, if a PDMS surface is oxidized at ambient temperature, stretching of this treated sample generates a series of parallel nanocracks with spacings in the order of a few microns [29–32]. The cracking is caused by the difference in mechanical properties of the silica-like films and the elastic PDMS substrate. The cracking phenomenon is similar to wrinkle formation and can be considered as an extreme case of the wrinkling process. The crack formation is reproducible in terms of average crack spacing, width and depth, which are mainly determined by the elastic moduli of the film and substrate, the thickness of the film and the stiffness of the system [29]. For example, the average crack spacing decreases with increasing applied strain, and the cracks are wider and deeper with larger applied stress. The formation of cracks is caused by irreversible plastic deformation. Therefore, the cracks do not completely close when the stretching is relieved, which means that the plasma-oxidation process induces a residual tension in the silica-like film. In ref. [30], the nanocracks are replicated into an ultraviolet-curable epoxy and PDMS prepolymer is cast against the epoxy mould to generate negative relief patterns of the cracks. Such a PDMS substrate is then sealed against an oxidized PDMS slab to form an array of enclosed nanochannels.

The geometry of such nanochannels is triangular or triangle like. As shown in the left part of Fig. 12c, by using the first method in Fig. 12a, wrinkles can be confined to specific regions on the PDMS surface for integration with other microfluidic devices [28]. Wrinkled nanochannels created by cover-plate bonding have triangular cross-sections (right part of Fig. 12c). Normally, the width/height is reduced in comparison with the original wavelength /amplitude of wrinkles owing to the bonding [28], which is beneficial for small nanochannel fabrication. However, van der Waals forces tend to enhance the adhesive attraction between wrinkles and substrate. The authors claimed that the height of the smallest nanochannels reliably produced was about 50 nm [28]. The nanochannels made by the second technique also assume the shape of a triangular cross-section with a height below 100 nm, which can be tuned by elastic deformation [30].

2.2.2. Tunable fluidic nanochannels for particle and DNA manipulation

Control and manipulation of nano-objects such as quantum dots, nanoparticles, and molecules have emerged as important processes for nanotechnology. A fluidic flow through nanochannels enables nano-objects or molecules to be controlled by an external mechanical force. For example, the flow of charged molecules or ions in a fluidic channel can be well controlled by applying a gate bias [33]. In daily life, we can control the water flow by reducing the size of the cross-section of the channel. On the nanoscale, the size control of nanochannels can be employed to manipulate nano-objects and molecules. However, the design and fabrication of such tunable nanochannels are challenging due to difficulties in controlling their uniformity and physical/chemical surface properties. Huh et al. reported that nanoscale cracks in oxidized PDMS (see Fig. 12b in Section 2.2.1) can actively manipulate fluidic transport by dynamic modulation of the channel cross-section [30]. The required deformation was achieved by applying relatively small external forces (22–42 kPa) to nanochannels with heights $>78 \pm 18$ nm. When a small force (22 kPa) was applied, quantum dots with diameters of 35 nm were completely obstructed, while small molecules (sulphorhodamine-101) passed through the channels with low flow rate. Pressing with 42 kPa caused the elastic nanochannels to be totally closed and the molecules stopped flowing as well. Such deliberate nanochannel constriction can also trap and release single nanoparticles [30]. As shown in Fig. 13a, a quantum dot (diameter $\sim$20 nm) moved from top to bottom when there was no compressive force. When deformed by 42 kPa, the nanochannel trapped the quantum dot as shown in Fig. 13b. Subsequent relief of the force enabled the quantum dot to continuously move down the channel (in c). Such mechanical handling of nano-objects offers a simple and universal way for the control and manipulation of small objects including nanoparticles as well as DNA molecules [34]. For example, single λ-phage DNA (48.5 kbp) was stretched from 30% to more than 70% of its fully stretched length by closing the nanochannels by pressing [30]. Fluidic stretching of DNA in such tunable nanochannels provides a new possibility for molecule linearization and could offer a new platform to investigate dynamics of DNA and other biopolymers at the single-molecule level.

2.3. Wrinkled surfaces as micro/nanofluidic templates and sieves

2.3.1. Basic principles of wrinkled templates and sieves

In Section 2.2.2, single nano-objects and molecules are controllably manipulated in fluid by tunable uniform nanochannels made from wrinkling-induced nanocracks. However, the

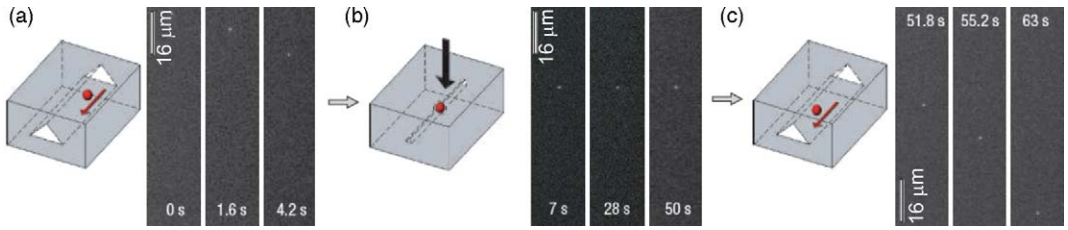

Fig. 13. (a) A single 20 nm quantum dot travelling along a relaxed nanochannel. Quantum dots are suspended in an aqueous bovine serum albumin solution (10 mg ml^{-1}). (b) Channel deformation at 42 kPa traps the particle. (c) Release of applied force resumes the flow of carrier liquid and the motion of the quantum dot [30]. Reprinted with permission from Macmillan Publishers Ltd.: *Nature Nanotechnology* [30], copyright (2007).

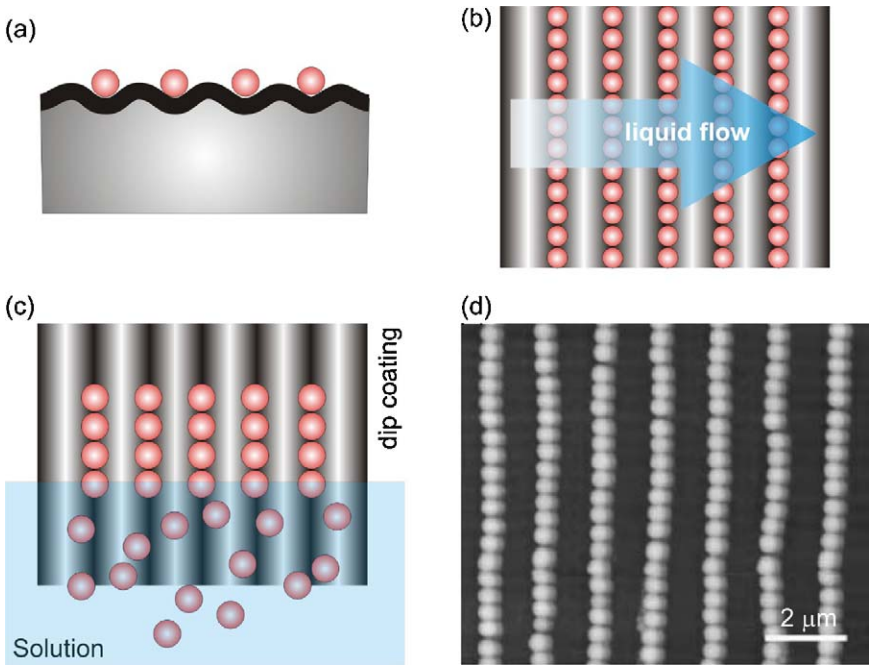

Fig. 14. (a) A sketch showing particles or colloids sitting in the trenches of wrinkles. Self-assembly of colloids by (b) liquid flowing and (c) dip coating. (d) Atomic force microscopy image of selective deposition of 380 nm-sized colloidal particles on $(PAH\text{-}PSS)_n$ wrinkled films [37].

assembly of nanoscale objects and molecules into long-range ordered patterns still holds a number of challenges. One possibility is to guide the self-assembly process by using patterned surfaces, which can be simply achieved by the wrinkling process as we described above. Since the periodicity and size of wrinkled patterns span across a multitude of length scales (from meter to nanometer), such patterns might constitute effective sieves for micro and nanoparticles [35].

As presented in Fig. 14a, a wrinkled surface of sinusoidal topography provides a geometric confinement for a colloid assembly due to the grooves. Two basic methods are applied to align the colloids: liquid flow (Fig. 14b) [35,36] and dip coating (Fig. 14c) [37,38]. In the dip-coating case, the withdrawing direction is aligned parallel to the wrinkle grooves. It is also expected that the deposition geometry of colloids is easily manipulated by using different wrinkles with controlled wavelengths and amplitudes. In Fig. 14d, chains of closely packed colloids 380 nm in diameter are formed in the wrinkled surface. More lines of colloids are packed in the wrinkles with longer wavelengths. In ref. [37], the authors claimed that the periodicity and geometry of the deposited colloid chains were determined by the employed templates with different wrinkle wavelengths. However, it is also mentioned that the aligned colloid chains have almost the same height above the template for different lines of colloids. Since the colloid assembly on wrinkles depends much on the resistance by the raised parts of wrinkles, the alignment phenomenon seems more related to the amplitude than the wavelength of the wrinkles. Nevertheless, the wavelength and amplitude are interrelated in this system. Hence, it should be interesting to model the process and find out which one is the intrinsic reason for "the same height".

By using an alterative method – spin coating, Horn et al. achieved a controllable alignment of tobacco mosaic virus (TMV) on wrinkled PDMS substrates [38]. Such well-aligned TMV arrays may serve as a model system for the alignment of anisotropic nano-objects or as metallization or mineralization templates for synthesis of aligned metal nanowires. Spin coating combines features from both dip coating and liquid flow. However, dip coating is better suited to guide the self-assembly of colloids because it operates closer to equilibrium conditions.

Wrinkled templates can act as sieves, selecting colloids with sizes corresponding to the wrinkle geometry. Researchers have developed multichannel sieves by using self-similar (or hierarchical) wrinkles [35], which are fabricated by a similar way to the first

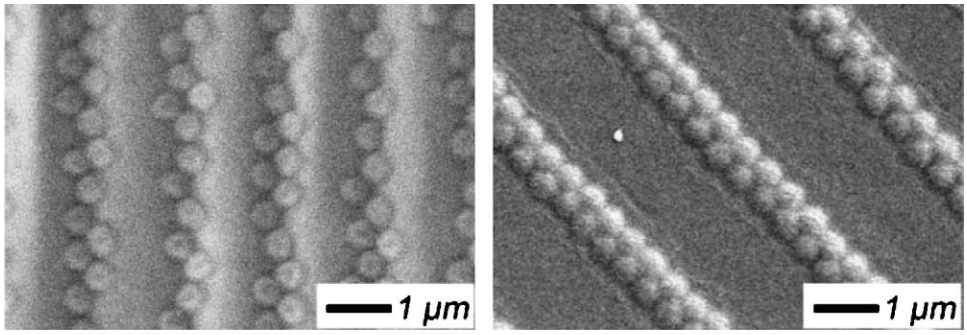

Fig. 15. SEM images showing (left) the deposition of PNIPAm colloids and (right) their transfer to a flat surface. Mechanical stretching and releasing the strain was used for the transfer [39].

method in Section 2.2.1. However, the heating and cooling steps are replaced by stretching and releasing. The releasing rate of oxidized PDMS substrates is the key for such nested self-similar wrinkles, where several distinct wrinkle generations are observed with wavelengths ranging from several tens of nanometers to half a millimeter. Such wrinkles of various wavelengths act as hosts for particles with different diameters under a constant liquid flow. In ref. [35], a triphasic aqueous suspension comprising particles with diameters of 67 nm, 3 μm, and 10 μm were chosen for the separation experiments by using the hierarchical wrinkles with wavelengths of ~50 nm, ~1 μm, ~5 μm, ~50 μm, and ~0.4 mm. It was found that 67 nm particles are collected by the 1-μm-wavelength wrinkles, those of 3 μm prefer to stay with 5-μm-wavelength wrinkles, and most of the 10-μm particles were collected by the grooves of the 50-μm-wavelength wrinkles. Such orientated segregation also works with lipid bilayers. Hierarchical wrinkles with nano to micrometer scale curvatures induce mesoscopic and molecular-level reorganizations, which may enable wrinkling capability in curvature-dependent biophysical processes [36].

2.3.2. Reversible wrinkling for controllable transfer of colloidal patterns

By using wrinkled patterns, colloids or particles can be well assembled into two- or three-dimensional geometries with defined orientations, shapes, and sizes. Hyun et al. suggested a reversible wrinkling or buckling process as a general approach for the recyclable loading-and-transfer of colloid patterns [39]. The first scheme in ref. [39] illustrates the experimental cycle of colloid loading on a wrinkled surface, transfer of the colloids to a flat surface, and replication of the initial wrinkling for recycling. The basic principle is similar to Section 2.3.1 for assembling colloids in trenches. The key is the reduction in the amplitude of the wrinkling patterns to a few nanometers as well as the recovery of the initial wrinkling patterns after transfer. There are two ways for the reversible change of the amplitude: (i) increase the amplitude by heating and reduce the amplitude by cooling; (ii) release the stretched layer for the large amplitude and re-stretch for lower amplitude for transfer. Such methods are universal since various colloidal particles like hydrogel, gold nanoparticles, and magnetic nanoparticles have been employed [39]. The left image of Fig. 15 shows the deposition of poly(*N*-isopropylacrylamide) (PNIPAm) colloids (400 nm in diameter) in the troughs of the wrinkled patterns, while the right image shows the transferred colloidal patterns onto a flat surface. By controlling the wrinkling periodicity and amplitude, different types of colloidal patterns are well replicated onto flat surfaces. Embossing of the colloids by reducing the wrinkle amplitude enabled the transfer of colloids regardless of their size and their layer thickness.

3. Wrinkling for mechanical characterization at micro/nanoscales

3.1. Buckling-based metrology

Wrinkle formation by buckling of compressively strained film can be used as a 'tool' to characterize the mechanical properties of the film itself [40–51]. In 2004, Stafford et al. have proposed and demonstrated an efficient way to measure the elastic modulus of nanoscale polystyrene (PS) films on PDMS substrates [40–42]. This method is based on a combination of laser light scattering from the buckled film and simultaneous application of compressive strain beyond the buckling stability of the film (see Fig. 16). For this measurement, the nanoscale film is supported by a thick PDMS substrate. PDMS is selected in this case because of its transparency and softness (very low elastic modulus). Due to the thin film (<300 nm), laser light is easily transmitted and scattered light can be observed on the screen. Fig. 16a shows the basic principle of this method when uniaxial stress is applied and one-dimensional wrinkles are formed. A simple apparatus for stretching the film is shown in Fig. 16b. In case of the one-dimensional wrinkle pattern, the distance between the diffraction spots observed on the screen are inversely proportional to the wavelength of the wrinkle λ according to Bragg's law. By proper calibration of this tool e.g. by AFM measurements, the wrinkle wavelength can be accurately determined. From buckling theory, it is well known that there is a critical wrinkle wavelength, when the energy of the film is minimized. This wavelength can be used to extract the reduced elastic modulus of the film ($\bar{E}_F = E_F/(1-\nu_F^2)$, where E_F and ν_F are Young's modulus and Poisson's ratio of the film, respectively.) by

$$\bar{E}_F = 3\bar{E}_S\left(\frac{\lambda}{2\pi d}\right)^3, \quad (1)$$

where d is the thickness of the film, $\bar{E}_S = E_S/(1-\nu_S^2)$ is the reduced elastic modulus of the substrate (PDMS in this case), and E_S (ν_S) is Young's modulus (Poisson's ratio) of the substrate. This method has been extended to estimate the modulus of two-dimensional buckling [41]. In this case, the difference in radius of each diffraction ring is inversely proportional to the wavelength of the wrinkle λ. Experimental examples of both one-dimensional and two-dimensional wrinkled films are shown in Fig. 16c–f. To date,

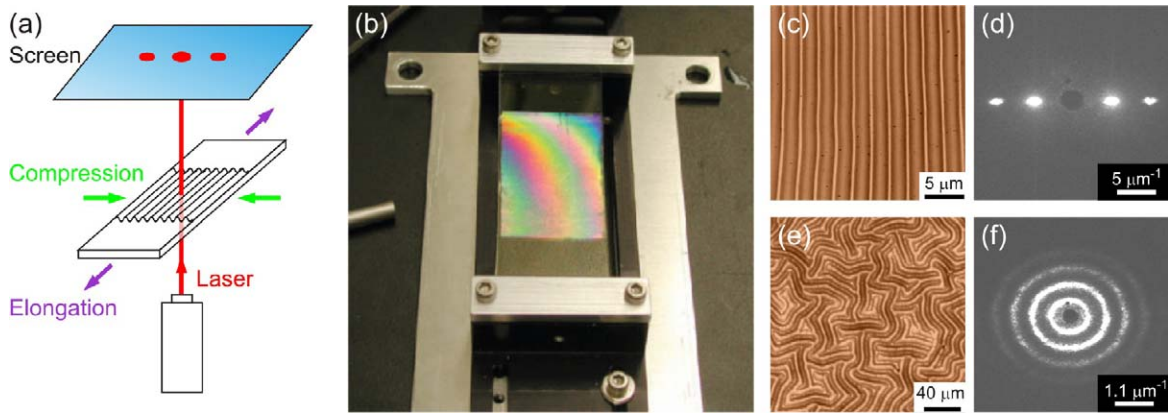

Fig. 16. (a) Schematic of small-angle light scattering instrument. (b) Photo of thin polymer film on PDMS substrate clamped between two supports. (c) Optical microscopy of one-dimensional buckling and (d) corresponding light scattering pattern [40]. Reprinted with permission from Macmillan Publishers Ltd.: *Nature Materials* [40], copyright (2004). (e) Optical microscopy of two-dimensional random buckling and (f) corresponding light scattering pattern. Note that the central light spots in (d) and (f) were blocked. Images are adapted from [41].

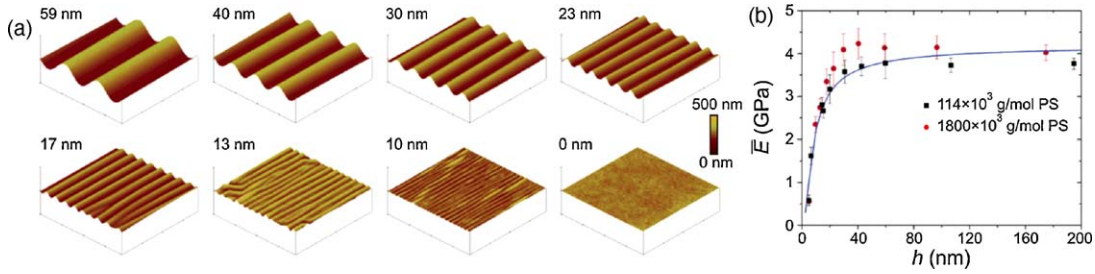

Fig. 17. (a) Set of perspective view AFM images of the buckling patterns of PS film with various film thickness. (b) The extracted reduced modulus $\bar{E}$ of the PS films for two different molecular weights. Images are adapted from [42]. Reprinted with permission from [42].Copyright 2006 American Chemical Society.

many polymer and organic films have been characterized by this technique [43,44].

The above method can be further extended to extract other related quantities of thin films. For instance, by observing the onset of wrinkle formation in real-time, the residue stress in the initial film can be measured [45]. Typical residue stresses of a few tens of MPa for PS films of a few hundred nanometer thickness have been reported. In addition, the cross-link density in ion-irradiated PS film can also be measured [46].

According to eq. (1), one can deduce that the wrinkle wavelength is linearly proportional to the thickness of a specific film type (with a constant modulus). However, when the polymer film is very thin (less than a few tens of nanometers), the elastic modulus is expected to be smaller than the bulk value. Fig. 17a shows a series of AFM images of wrinkled PS films to test this expectation [42]. By calculating the reduced elastic modulus from the measured wavelength and the thickness using eq. (1), the apparent Young's modulus shows a clear reduction when the film is thinner than 40 nm. This value is independent of the molecular weight of the PS films. This evidence is consistent with results obtained from other measurement techniques and molecular dynamic atomistic simulations.

Wrinkle formation as a tool to determine the elastic modulus has been extended to multilayer films [42]. Fig. 18 shows a schematic illustration of the buckling of a bilayer film as compared to the single layer. For the bilayer, the effective modulus depends on the elastic modulus of both layers and the thickness ratio between them. By the elastic theory, it is known that the effective modulus of the bilayer is

$$\bar{E}_F = \frac{d_1^4\bar{E}_1^2 + 2d_1d_2(2d_1^2 + 3d_1d_2 + 2d_2^2)\bar{E}_1\bar{E}_2 + d_2^4\bar{E}_2^2}{(d_1+d_2)^3(d_1\bar{E}_1 + d_2\bar{E}_2)}, \quad (2)$$

where $\bar{E}_{1,2}$ ($d_{1,2}$) is the reduced modulus (thickness) of the layer no. 1 and 2. If the modulus of one layer is known, the other modulus can be extracted from measurement. The solid line in Fig. 17b is the fit of experimental data by assuming two layers of PS films (with different elastic modulus and thickness).

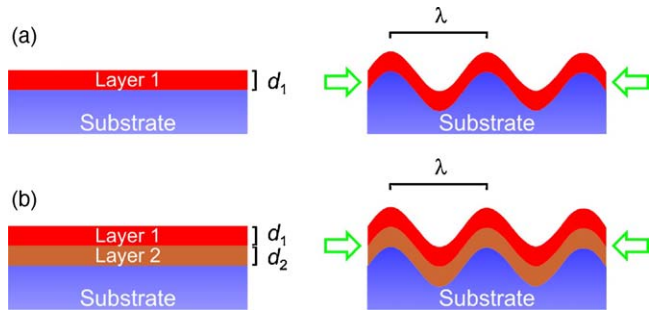

Fig. 18. Cross-sectional illustration of unstrained and strained (a) single layer and (b) bilayer. The layers undergo buckling states with characteristic wavelength when the strain is beyond the critical value.

In addition to the analysis of wrinkled two-dimensional films, the idea to determine the elastic modulus from buckling of wires and tube structures has also been proposed [47]. In the work of Cao et al. [47], buckling of different cross-sectional shapes has been modeled using large-scale finite-element method. This theoretical modeling is still waiting for experimental confirmation.

3.2. Capillary wrinkling

Another method to characterize thin film properties is by observing wrinkle pattern formation during capillary force interaction with thin films. This is a rather simple method, which requires a dish of fluid and a low magnification microscope [52]. As demonstrated by Huang et al., by putting a liquid droplet onto a thin film wrinkles can form with the wrinkle length and period following a simple law. In Fig. 19, the water droplets are used to test the PS film placed on water. The number of wrinkles formed around the drop can be described by

$$N \propto \left[\frac{\gamma(1-\nu_F^2)}{E_F}\right] a^{1/2}h^{-3/4}, \quad (3)$$

where γ is the surface tension at the boundary of the drop, a is the radius of the drop and h is the thickness of the film. This capillary wrinkling can be used to measure and correlate elasticity and thickness of the film as well as the dynamical relaxation in ultrathin films [52].

4. Wrinkling as a new feature in nanostructures

4.1. Wrinkled one-dimensional nanostructures

Chemical-modifications are often adopted to functionalize the surfaces of nanostructures. For example, a silicon nanomembrane with a chemically modified rough surface reveals a persistent photoconductivity, which is three orders of magnitude higher than that of previous reports without chemical modifications [53]. Recently, physically wrinkled (or buckled) single carbon nanotubes (CNTs) and Si nanowires (SNWs) have been achieved by embedding CNTs or SNWs onto pre-strained PDMS surfaces. By releasing such structures, individual wrinkled CNTs or SNWs are formed. However, different wrinkles for CNTs and SNWs are reported in refs. [54,55]. As seen in Fig. 20, wrinkles of CNTs assume sinusoidal shapes out of the plane, but SNWs on the PDMS surfaces wrinkle up in the plane. This dissimilarity was attributed to the difference of mechanical properties between CNTs and SNWs, which is interesting since such method can be applied to other similar types of materials, such as DNA and RNA. The experimental procedures and theoretical analysis provide a simple route to measure the linear elastic properties of such one-

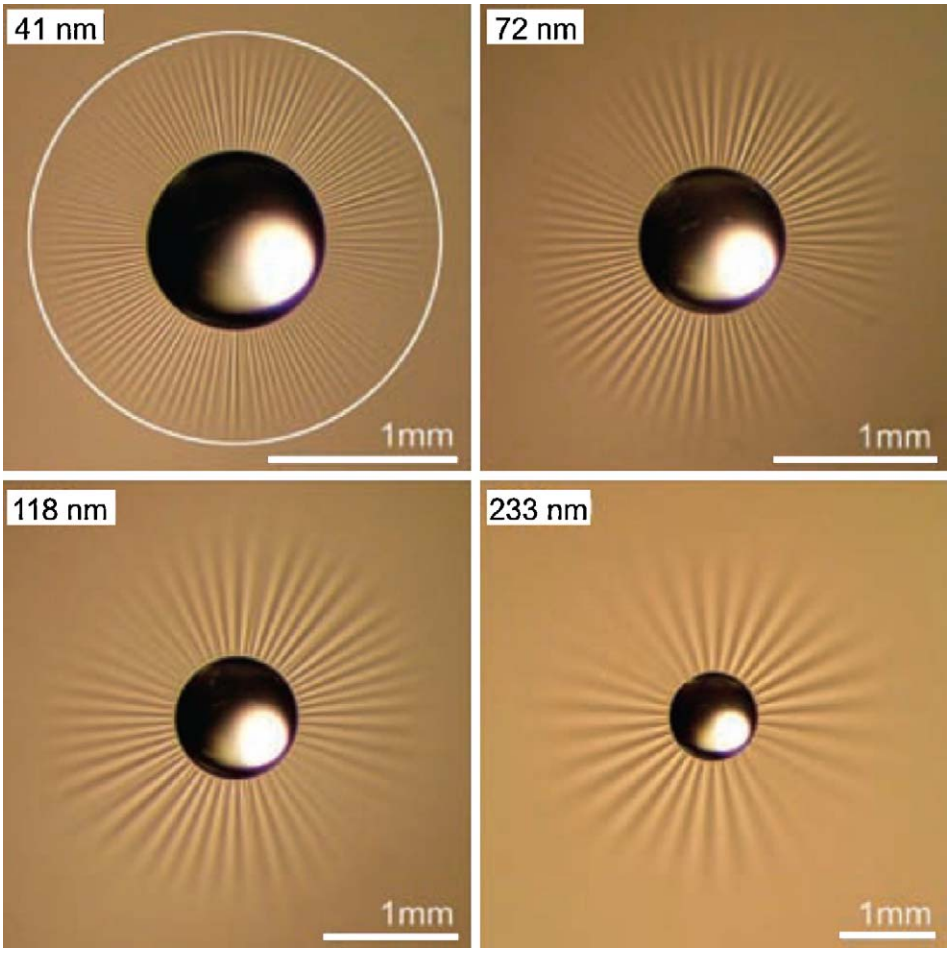

Fig. 19. Demonstration of wrinkle formation by capillary force on interface between water droplet and thin film. Thicknesses indicated on the upper left of each image influence both the wrinkle length and wrinkle period. Images are adapted from [52]. Reprinted with permission from AAAS.

dimensional nanostructures [55–56]. Wrinkling processes involve strain modifications of nanostructures, which offers an opportunity to study their strain coupling to electronic properties for potential applications such as strain gauge devices.

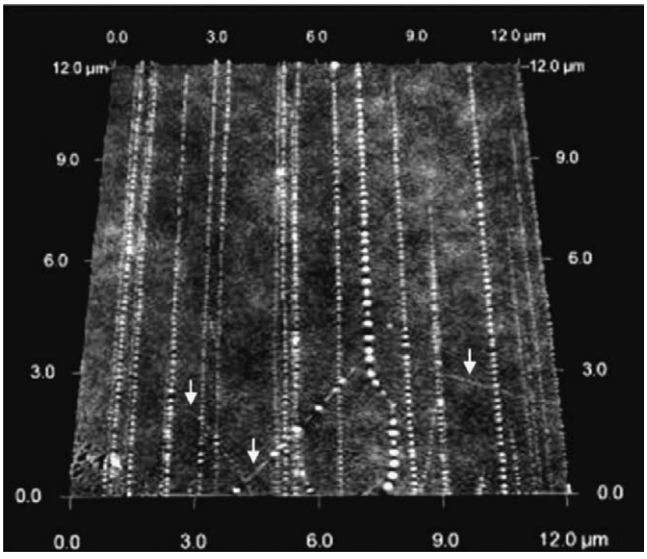

Fig. 20. Angled-view atomic force microscopy image of wavy single-walled CNTs on a PDMS substrate [54]. Reprinted with permission from [54].Copyright 2008 American Chemical Society.

The realization of thin layers containing nanostructures like CNTs suggests interesting applications in e.g. conductors, sensors [57] and energy storage devices [58]. A recent review on ultrathin films and wrinkling of single-walled CNTs has been published by Cao and Rogers [57]. Recently, Yu et al. have constructed stretchable supercapacitors based on wrinkled single-walled CNTs thin layers, and their electrochemical performance remains unchanged during mechanical stretching [58].

Besides, it has been found that wrinkled silver nanowires show surface-enhanced Raman scattering at the vicinity of the formed nano-wrinkles [59]. Previously, wrinkled polymer films containing gold particles or silver nanowires were fabricated by layer-by-layer method [60,61], and offered a possibility to imprint an array of nanostructures into flexible polymer supports for certain applications. Silver nanowires are wrinkled on a pre-strained PDMS substrate, and most of them experience a wide spread of periodicities. Such nano-wrinkles show interesting optical properties, such as photo-plasmon conversion and emission from subwavelength structures. Jiang et al. demonstrated that the enhancement of Raman signals can be modulated by the presence of silver nano-wrinkles.

4.2. Wrinkled-up graphene for strain-engineering

Wrinkling phenomena are always related to strain, which could be a possible method for bandgap engineering of graphene (a single layer of carbon atoms densely packed in a honeycomb crystal lattice) [1]. The words ‘ripples’ and ‘corrugations’ are

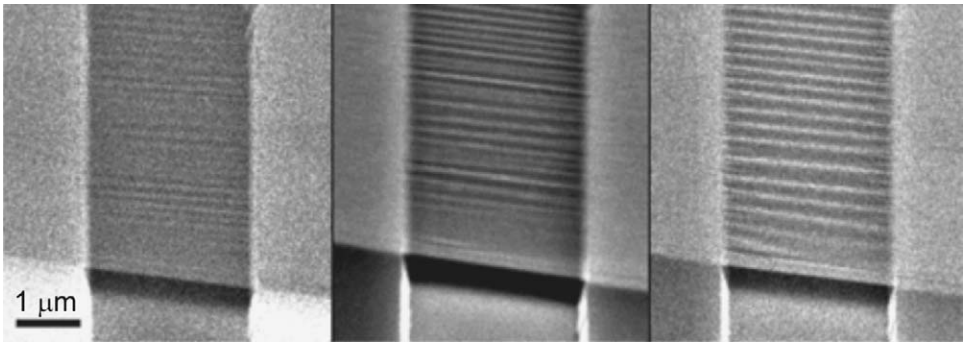

Fig. 21. SEM images of a graphene sheet before annealing (left), after annealing at 425 K (middle) and to 475 K (right) [1]. Note the increase in wavelength and amplitude of the wrinkles with annealing temperature. Reprinted with permission from Macmillan Publishers Ltd.: *Nature Nanotechnology* [1], copyright (2009).

literally used in many publications instead of wrinkles [62–66]. In 2007, Meyer et al. found that suspended graphene sheets are not perfectly flat and reveal an out-of-plane deformation of 1 nm [62]. This deformation is referred to as intrinsic ripples, which was theoretically investigated by Fasolino et al. [63]. In a further scanning tunneling microscopy study of a graphene sheet, a new class of wrinkles with ~10 nm width and ~3 nm height was observed [66]. Interestingly, such wrinkles have lower electrical conductance, suggesting that wrinkles might be important for understanding the electrical properties of graphene. Wrinkles in graphene can be formed by using some simple methods described below (see Fig. 21). For example, Li et al. have reported that wrinkled graphene nanostructures can be formed on soft substrates [65]. Periodic wrinkles with amplitudes of nanometer scale spontaneously appear at the edges of single-layer graphene after heating and cooling of samples. A molecular dynamics and continuum plate theory suggests that a circular single-layer graphene sheet deformed by nanoindentation can also form wrinkled patterns [64]. Very recently, Bao et al. have demonstrated a controllable method to develop wrinkled graphene sheets by thermally generated strains [1]. As shown in Fig. 21a, a free-standing graphene sheet with small wrinkles is observed before annealing. After annealing, wrinkles become more and more pronounced as the temperature increases (see Fig. 21b and c). In such experiments, one can control wrinkle orientations, wavelengths and amplitudes by adjusting boundary conditions and annealing temperatures since graphene has a negative thermal expansion coefficient [1]. The fabrication of all these wrinkled-up nanostructures is motivated by the opening of a bandgap in graphene due to the involved strain modifications. However, there seems no considerable change in the electronic properties even with a strain up to ~15% [1,67,68]. More exploration in both theory and experiments is required in future [68]. We believe that wrinkling could offer an important approach to understand strain-engineered electronic properties of graphene.

5. Conclusions and outlook

From a theoretical point of view, it is well known that the elastic energy of strained membranes can be efficiently relaxed by wrinkle formation (buckling phenomena), and classical continuum elasticity is commonly employed for membranes thicker than a few tens of nanometers. As extensively described in this review, the spontaneous buckling of micro/nanomembranes can even be controlled in exact geometry and position applying standard photolithographic techniques. However, the realization of more complicated architectures for practical integrated devices is not yet fully understood. In particular, the interaction of wrinkles with the substrate surface still poses great challenges for understanding pattern formation at solid–solid interfaces. Furthermore, wrinkling in monolayer thick membranes (including graphene sheets) is neither well understood nor well controlled. It is known that a two-dimensional atomic layer is not stable due to environmental fluctuations [63], and random wrinkling is always observed in such a film. Methods to control wrinkling in a few nanometers to sub-nanometer thin films will therefore require extensive future efforts – both theoretically and experimentally.

From a practical point of view, one of the most exciting and yet lacking devices are ionic field-effect transistors (i-FETs) [69,70] based on wrinkled nanochannels, although several interesting nanofluidic studies on wrinkles have been demonstrated as presented in Section 2. Highly integrative i-FETs are required for applications in e.g. separation science and energy conversion [69]. However, nanochannel fabrication methods are often limited to demonstrator devices without the capability for large-scale integration. I-FETs based on highly ordered wrinkled nanochannel networks [25] could in principle be upscaled and mass-produced on a chip.

In summary, we have summarized numerous principles of wrinkle formation on the micro and nanoscale with special emphasis on potential applications, such as fluidics, mechanics, etc. Micro and nano-fluidic studies are highlighted by using different types of wrinkles. Wrinkling as a mechanical characterization tool to extract the elastic properties of thin films is described. As a new feature, wrinkles are employed to modify the properties of nanostructured materials. It is also promising to apply wrinkling for strain-engineering of graphene. Based on the above and other interesting effects of wrinkles like microlenses [71,72], cell culture scaffolds [73], tunable or programmable optical devices [74,75], we believe that wrinkling of micro/nanostructures offers a fruitful research platform for future interdisciplinary progress in nanotechnologies.

Acknowledgements

We thank Christoph Deneke and Francesca Cavallo for experimental help. This work was financially supported by grants from the Volkswagen Foundation (I/84 072) and a Multidisciplinary University Research Initiative (MURI) sponsored by the U.S. Air Force Office of Scientific Research (AFOSR) Grant No. FA9550-09-1-0550. Partial support was also from Germany/Hong Kong Joint Research Scheme (Grant No. 426/hk-PPP-cab).

References

[1] W. Bao, F. Miao, Z. Chen, H. Zhang, W. Jang, C. Dames, C.N. Lau, Nat. Nano 4 (2009) 562.
[2] N. Bowden, S. Brittain, A.G. Evans, J.W. Hutchinson, G.W. Whitesides, Nature 393 (1998) 146.
[3] A. Schweikart, A. Fery, Microchim. Acta 165 (2009) 249.
[4] J. Genzer, J. Groenewold, Soft Mater. 2 (2006) 310.

[5] E. Cerda, L. Mahadevan, Phys. Rev. Lett. 90 (2003) 074302.
[6] S.Y. Chou, P.R. Krauss, P.J. Renstrom, Science 272 (1996) 85.
[7] Y.F. Mei, Z.M. Li, R.M. Chu, Z.K. Tang, G.G. Siu, R.K.Y. Fu, P.K. Chu, W.W. Wu, K.W. Cheah, Appl. Phys. Lett. 86 (2005) 021111.
[8] Y.F. Mei, G.G. Siu, Y. Yang, R.K.Y. Fu, T.F. Hung, P.K. Chu, X.L. Wu, Acta Mater. 52 (2004) 5051.
[9] Y.F. Mei, G.S. Huang, Z.M. Li, G.G. Siu, R.K.Y. Fu, Y.M. Yang, X.L. Wu, Z.K. Tang, P.K. Chu, Acta Mater. 52 (2004) 5633.
[10] G.M. Whitesides, B. Grzybowski, Science 295 (2002) 2418.
[11] H. Porada, E.H. Bouougri, Earth Sci. Rev. 81 (2007) 199.
[12] M.C. Cross, P.C. Hohenberg, Rev. Mod. Phys. 65 (1993) 851.
[13] Y. Sun, J.A. Rogers, Adv. Mater. 19 (2007) 1897.
[14] D.-H. Kim, J.A. Rogers, Adv. Mater. 20 (2008) 4887.
[15] D.-Y. Khang, J.A. Rogers, H.H. Lee, Adv. Funct. Mater. 19 (2009) 1526.
[16] Y. Sun, W.M. Choi, H. Jiang, Y.Y. Huang, J.A. Rogers, Nat. Nano 1 (2006) 201.
[17] D.-H. Kim, J.-H. Anh, W.M. Choi, H.-S. Kim, T.-H. Kim, J. Song, Y.Y. Huang, Z. Liu, C. Lu, J.A. Rogers, Science 320 (2008) 507.
[18] S.–i. Park, Y. Xiong, R.-H. Kim, P. Elvikis, M. Meitl, D.-H. Kim, J. Wu, J. Yoon, C.-J. Yu, Z. Liu, Y. Huang, K.-C. Hwang, P. Ferreira, X. Li, K. Choquette, J.A. Rogers, Science 325 (2009) 977.
[19] H.C. Ko, M.P. Stoykovivh, J. Song, V. Malyarchuk, W.M. Choi, C.-J. Yu, J.B. Geddes III, J. Xiao, S. Wang, Y. Huang, J.A. Rogers, Nature 454 (2008) 748.
[20] J.A. Rogers, IFW-Colloquium, Dresden, Germany, November 19, 2009.
[21] P. Cendula, S. Kiravittaya, Y.F. Mei, Ch. Deneke, O.G. Schmidt, Phys. Rev. B 79 (2009) 085429.
[22] Y.F. Mei, D.J. Thurmer, F. Cavallo, S. Kiravittaya, O.G. Schmidt, Adv. Mater. 19 (2007) 2124.
[23] Y.F. Mei, S. Kiravittaya, M. Benyoucef, D.J. Thurmer, T. Zander, Ch. Deneke, F. Cavallo, A. Rastelli, O.G. Schmidt, Nano Lett. 7 (2007) 1676.
[24] A. Malachias, Y.F. Mei, R.K. Annabattula, C. Deneke, P.R. Onck, O.G. Schmidt, ACS Nano 2 (2008) 1715.
[25] S. Harazim, P. Feng, Y.F. Mei, Ch. Deneke, O. G. Schmidt, unpublished.
[26] M. Ouyang, R.J. Muisener, A. Boulares, J.T. Koberstein, J. Membr. Sci. 177 (2000) 177.
[27] N. Bowden, W.T.S. Huck, K.E. Paul, G.M. Whitesides, Appl. Phys. Lett. 75 (1999) 2557.
[28] S. Chung, J.H. Lee, M.-W. Moon, J. Han, R.D. Kamm, Adv. Mater. 20 (2008) 3011.
[29] X. Zhu, K.L. Mills, P.R. Peters, J.H. Bahng, E.H. Liu, J. Shim, K. Naruse, M.E. Csete, M.D. Thouless, S. Takayama, Nat. Mater. 4 (2005) 403.
[30] D. Huh, K.L. Mills, X. Zhu, M.A. Burns, M.D. Thouless, S. Takayama, Nat. Mater. 6 (2007) 424.
[31] K.L. Mills, X. Zhu, S. Takayama, M.D. Thouless, J. Mater. Res. 23 (2008) 37.
[32] T. Uchida, K.L. Mills, C.-H. Kuo, W. Roh, Y.-C. Tung, A.L. Garner, K. Koide, M.D. Thouless, S. Takayama, Langmuir 25 (2009) 3102.
[33] R. Fan, M. Yue, R. Karnik, A. Majumdar, P. Yang, Phys. Rev. Lett. 95 (2005) 086607.
[34] N. Douville, D. Huh, S. Takayama, Anal. Bioanal. Chem. 391 (2008) 2395.
[35] K. Efimenko, M. Rackaitis, E. Manias, A. Vaziri, L. Mahadevan, J. Genzer, Nat. Mater. 4 (2005) 293.
[36] B. Sanii, A.M. Smith, R. Butti, A.M. Brozell, A.N. Parikh, Nano Lett. 8 (2008) 866.
[37] C. Lu, H. Möhwald, A. Fery, Soft Matt. 3 (2007) 1530.
[38] A. Horn, H.G. Schoberth, S. Hiltl, A. Chiche, Q. Wang, A. Scherikart, A. Fery, A. Böker, Faraday Discuss. 143 (2009) 143.
[39] D.C. Hyun, G.D. Moon, E.C. Cho, U. Jeong, Adv. Funct. Mater. 19 (2009) 2155.
[40] C. Stafford, C. Harrison, K.L. Beers, A. Karim, E.J. Amis, M.R. Vanlandingham, H.-C. Kim, W. Volksen, R.D. Miller, E.E. Simonyi, Nat. Mater. 3 (2004) 545.
[41] C.M. Stafford, S. Guo, C. Harrison, M.Y.M. Chiang, Rev. Sci. Instrum. 76 (2005) 062207.
[42] C.M. Stafford, B.D. Vogt, C. Harrison, D. Julthongpiput, R. Huang, Macromolecules 39 (2006) 5095.
[43] J.M. Torres, C.M. Stafford, B.D. Vogt, ACS Nano 3 (2009) 2677.
[44] D. Tahk, H.H. Lee, D.-Y. Khang, Macromolecules 42 (2009) 7079.
[45] J.Y. Chung, T.Q. Chastek, M.J. Fasolka, H.W. Ro, C.M. Stafford, ACS Nano 3 (2009) 844.
[46] Y. Karade, S.A. Pihan, W.H. Brünger, A. Dietzel, R. Berger, K. Graf, Langmuir 25 (2009) 3108.
[47] Y.-P. Cao, X.-P. Zheng, B. Li, X.-Q. Feng, Scripta Mater. 61 (2009) 1044.
[48] J.-L. Sormana, S. Chattopadhyay, J.C. Meredith, Rev. Sci. Instrum. 76 (2005) 062214.
[49] A.J. Nolte, M.F. Rubner, R.E. Cohen, Macromolecules 38 (2005) 5367.
[50] A.J. Nolte, R.E. Cohen, M.F. Rubner, Macromolecules 39 (2006) 4841.
[51] C. Jiang, X. Wang, R. Gunawidjaja, Y.-H. Lin, M.K. Gupta, D.L. Kaplan, R.R. Naik, V.V. Tsukruk, Adv. Funct. Mater. 17 (2007) 2229.
[52] J. Huang, M. Juszkiewicz, W.H. De Jeu, E. Cerda, T. Emrick, N. Menon, T.P. Russell, Science 317 (2007) 650.
[53] P. Feng, I. Mönch, S. Harazim, G.G. Huang, Y.F. Mei, O.G. Schmidt, Nano Lett. 9 (2009) 3453.
[54] D.-Y. Khang, J. Xiao, C. Kocabas, S. MacLaren, T. Banks, H. Jiang, Y.Y. Huang, J.A. Rogers, Nano Lett. 8 (2008) 124.
[55] S.Y. Ryu, J. Xiao, W.I. Park, K.S. Son, Y.Y. Huang, U. Paik, J.A. Rogers, Nano Lett. 9 (2009) 3214.
[56] J. Xiao, H. Jiang, D.-H. Khang, J. Wu, Y. Huang, J.A. Rogers, J. Appl. Phys. 104 (2008) 033543.
[57] Q. Cao, J.A. Rogers, Adv. Mater. 20 (2008) 1.
[58] C. Yu, C. Masarapu, J. Rong, B. Wei, H. Jiang, Adv. Mater. (2009), doi:10.1002/adma.200901775.
[59] N.L. Netzer, R. Gunawidjaia, M. Hiemstra, Q. Zhang, V.V. Tsukruk, C. Jiang, ACS Nano 3 (2009) 1795.
[60] R. Gunawidjiajia, H. Ko, C. Jiang, V.V. Tsukruk, Chem. Mater. 19 (2007) 2007.
[61] C. Jiang, S. Singamaneni, E. Merick, V.V. Tsukruk, Nano Lett. 6 (2006) 2254.
[62] J.C. Meyer, A.K. Geim, M.I. Katsnelson, K.S. Novoselov, T.J. Booth, S. Roth, Nature 446 (2007) 60.
[63] A. Fasolino, J.H. Los, M.I. Katsnelson, Nat. Mater. 6 (2007) 858.
[64] C.Y. Wang, K. Mylvaganam, L.C. Zhang, Phys. Rev. B 80 (2009) 155445.
[65] Z. Li, Z. Cheng, R. Wang, Q. Li, Y. Fang, Nano Lett. 9 (2009) 3599.
[66] K. Xu, P. Cao, J.R. Heath, Nano Lett. (2009), doi:10.1021/nl902729p.
[67] C. Lee, X. Wei, J.W. Kysar, J. Hone, Science 321 (2008) 385.
[68] F. Guinea, M.I. Katsnelson, A.K. Geim, Nat. Phys. 6 (2009) 30.
[69] W. Sparreboom, A. van den Berg, J.C.T. Eijkel, Nat. Nanotech. 4 (2009) 713.
[70] R. Fan, M. Yue, R. Karnik, A. Majumdar, P. Yang, Phys. Rev. Lett. 95 (2005) 086607.
[71] E.P. Chan, A.J. Crosby, Adv. Mater. 18 (2006) 3238.
[72] D. Chandra, S. Yang, P.-C. Lin, Appl. Phys. Lett. 91 (2007) 251912.
[73] X. Jiang, S. Takyama, X. Qian, E. Ostuni, H. Wu, N. Bowden, P. LeDuc, D.E. Ingber, G.M. Whitesides, Langmuir 18 (2002) 3273.
[74] C. Harrison, C.M. Stafford, W. Zhang, A. Karim, Appl. Phys. Lett. 85 (2004) 4016.
[75] C.W. Brown, G.G. Wells, M.I. Newton, G. McHale, Nat. Photonics 3 (2009) 403.